Phase Transformations and Dislocations Mechanisms of $Al_{0.3}CoCrFeNi$ High Entropy Alloy: A Nanoscale Investigation

Dheyaa F. Kadhim[1,a)]

[1] *Department of Mechanical Engineering, University of Thi-Qar, Iraq*
[a)] Corresponding author: *Dheyaa.kadhim@utq.edu.iq*

ABSTRACT

In the present investigation, the change of phase transition, the mechanism of dislocation, and the mechanical characteristics of the $Al_{0.3}CoCrFeNi$ high-entropy alloy was examined using molecular dynamics simulations. The affecting variables, such as temperature and strain rate, have been taken into account. The findings reveal that the phase transitions from the original single face-centered cubic form to hexagonal close-packed, body-centered cubic and amorphous phase as the strain develops. In particular, this change happens following the yield strain. $Al_{0.3}CoCrFeNi$ HEA's compressive characteristics are negatively impacted by temperature rise. The shear strain advances as the temperature raises and is distributed uniformly while the dislocation density decrease. In contrast, the yield stresses of high-entropy alloys climb noticeably when the strain rate rises. With rising temperatures, the dislocation density rises. Additionally, the process of phase change is critical for stacking defects. The findings offer a fundamental insight of plastic deformation in $Al_{0.3}CoCrFeNi$ HEA and are qualitatively compatible with experiments.

Keywords: Al0.3CoCrFeNi High-Entropy Alloys, Multi-component Alloys, Molecular Dynamics Simulation, Nanoscale FCC to HCP phase transformations

1. Introduction

In contrast to ordinary alloys, which only comprise one or two basic elements, high entropy alloys (HEAs) are a brand-new class of materials. HEAs typically include more than four key components. Due to the fact that under two circumstances, the entropy is noticeably higher, the term has previously been coined. One is when more important components are present, and the other is when their ratios are almost equal. great strength and hardness, great thermal stability, and exceptional corrosion resistance are characteristics of HEAs. However, it is extremely fragile. Most HEAs have either face-centered cubic (FCC) or body-centered cubic (BCC) lattice crystal structures. While HEAs with FCC structures have more mobility with lower strength, HEAs with BCC structures have poor fluidity and high strength. When considering the unique uses and cost-effective alloy, the selection of materials for HEAs is crucial[1].

Numerous HEA systems have recently been used, and the majority of study has concentrated on the microstructure and characteristics of the AlxCoCrFeNi HEAs system. [1]. In contrast to traditional alloys, HEAs offer superior thermal stability, excellent fatigue, wear, and corrosion resistance, improved hardness, and exceptional elevated and cryogenic temperature properties, according to recent studies. These qualities make HEAs suitable candidates to fulfill stringent requirements for specialized severe applications, especially in the nuclear, turbine, and aircraft sectors.[2]. One of the first high-entropy alloys to be explored was AlxCoCrFeNi, and it is currently one of the most widely used.

The AlCoCrFeNi alloy's mechanical characteristics and the effects of different elemental concentrations on those characteristics are frequently studied by researchers. [3-9]. The HEAs also possess numerous outstanding mechanical qualities, including high strength, high wear resistance, high plasticity, corrosion resistance, and great performance at both cryogenic and high temperatures. [10].

Since the $Al_{0.3}$CoCrFeNi alloy has undergone extensive experimental study, it was chosen for this work. However, there aren't many investigations on the AlxCoCrFeNi HEA's nanoscale deformation mechanisms.[11-13]. To the best of our knowledge, however, no research has been done on the nanoscale phase change and strengthening mechanisms of Al0.3CoCrFeNi. The exploration of the microstructure, thermodynamics, and mechanical characteristics using molecular dynamics (MD) is an effective method for gaining a nanoscale understanding of the deformation behaviors of materials. The strategy is to use a collection of parameterized functions and a semi-empirical interatomic potential to depict a material's potential-energy hypersurface. In the simulations, an accurate interatomic potential is essential. The modified embedded atom method (EAM), which exhibits a variety of elements within various structures using the same mathematical formalization, is the optimal interatomic-potential model for Al0.3CoCrFeNi HEA.[14].

In this study, MD simulations were used to examine how temperature and strain rate affected the development of the microstructure, mechanical characteristics, and phase transition process of nanocrystalline $Al_{0.3}$CoCrFeNi HEA. We've talked about the radial distribution function (RDF), atomic structure, and dislocation evolution. In order to examine the phase of HEA thin, the local atomic structures were determined and described by calculating the radial distribution functions (RDF). The usefulness of MD simulations to forecast phase transformations in Al0.3CoCrFeNi HEA was proven by comparison with the experimental data that is currently accessible.

2. Computational Method

2.1. Simulation Method

Simulation is done using (LAMMPS) molecular dynamics code [15] Relaxation is first put into practice. The relaxation can be accomplished in two steps: first, the solid solution Al0.3CoCrFeNi HEA system is submitted to canonical ensemble at 250 K for 150 ps , and second, by using the isothermal-isobaric ensemble at 250 K for 200 ps. When balance is established, the relaxation is complete. Next, an NPT ensemble with a pressure being set to zero is used to apply strain rates of $1x\ 10^{-2}\ s^{-1}$ along the z-direction. Compressive loads are applied along the z-direction under a time step of 1 femtosecond (fs). Periodic boundary conditions is utilized along with the Verlet velocity algorithm [14].

2.2. Interatomic potential

The embedded-atom-method (EAM) potential created by Daw et al .[16] since it can demonstrate a variety of elements within variations in structure using the same mathematical framework, has been frequently used for HEAs to accurately replicate the mechanical and structural properties of materials. [17-19]. We applied an EAM potential function in the current research that was presented by Farkas et al. [20].

2.3. Simulation setup

Al(green), Cr(red), Co(yellow), Fe(violet), and Ni(blue) atoms are randomly distributed in a (15a 15a 15a) nm3 FCC lattice as represented in Figure 1, where the lattice constant, a = 0.359 nm as calculated in our previous paper [21]. is used to create a simulation domain, making up 62,500 atoms. All directions are subject to periodic boundary conditions. Visualization Tool for Open Source (OVITO) [22] is used to post-process molecular trajectories using Common Neighbor Analysis (CNA)[23], Centrosymmetry Parameter (CSP) analysis [24], and Dislocation Analysis (DXA) [25].

The structure is then initiated at 1870 K in an (NPT) ensemble for 90 ps at a pressure of 0 MPa. The alloy is quickly cooled to 250 K, and the structure is then allowed to equilibrate for an additional 90 ps. The quenched HEA is then repeatedly simulated for 10 ps under the Nóse-

Hoover. The structure is allowed to equilibrium for 10 ps to complete the procedure of quenching under the (NVE) ensemble.

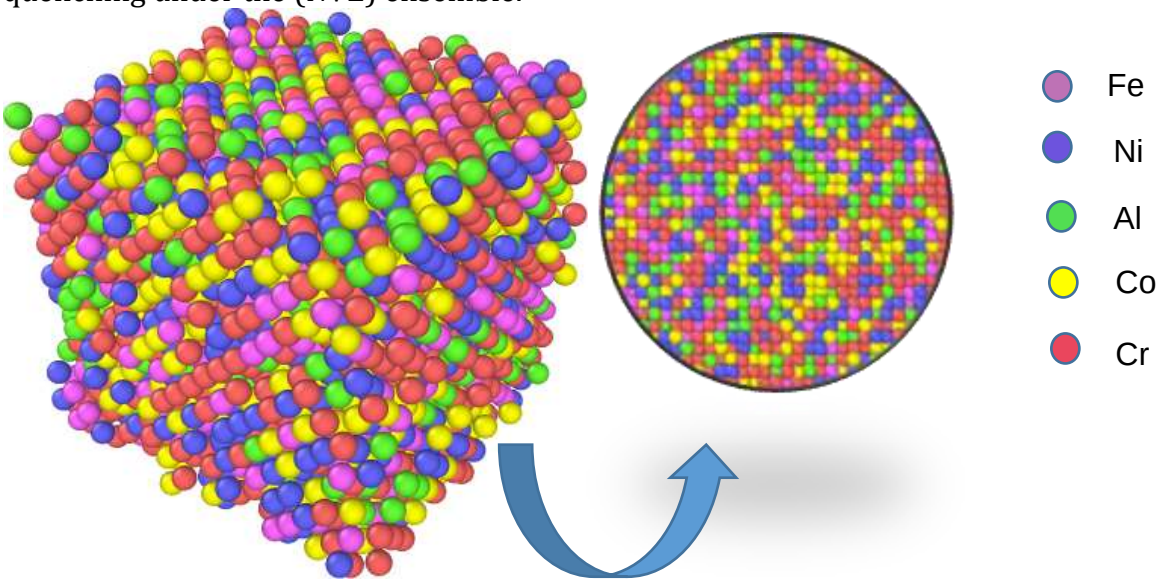

Figure 1. Represents the MD model of FCC nanostructured $Al_{0.3}$CoCrFeNi HEA.

3. Results and Discussions

3.1 Evaluation of Microstructures

A great deal of research has been done on the physical, chemical, and mechanical characteristics of alloys such AlxCoCrFeNi high-entropy alloy [26, 27].]. However, there have not been many reports of the computational compression properties. Experimental evidence suggests that the face-centered cubic crystal structure of $Al_{0.3}$CoCrFeNi alloy. Figure 2 (b) shows ® findings regarding the undeformed alloy. We discover that the two main crystalline phases in the alloy are the FCC (61%) and disordered coordination (39%). The remaining phases are only present in marginal amounts: BCC is 9.3% and hexagonal close packed (HCP) is about 12.2.8%. The usual FCC verification of a lattice is depicted by peaks along nearest neighbors atoms that are spaced apart at specific intervals, which is consistent with experimental results, is reproduced by the average of all atom pairs to produce the structural pair function, and shown in Figure 2 (a). Our selection of the molecular dynamics lattice structure and potential function are therefore verified, enabling predictive assessments of the $Al_{0.3}$CoCrFeNi HEA deformation mechanisms that had previously only been possible through experimental research. According to Wang et al. report, the columnar FCC phase in the as-cast high entropy exists [28]. Additionally, Kaoa et al. demonstrated that the Al0.3CoCrFeNi crystal structure is FCC [26]. It was believed that the creation of a single solution rather than intermetallic phases in such alloys was caused by entropy and slow effects, which lower the Gibbs energy [29]. Numerous researches have indicated that $Al_{0.3}$CoCrFeNi is made up of a single FCC phase.

.

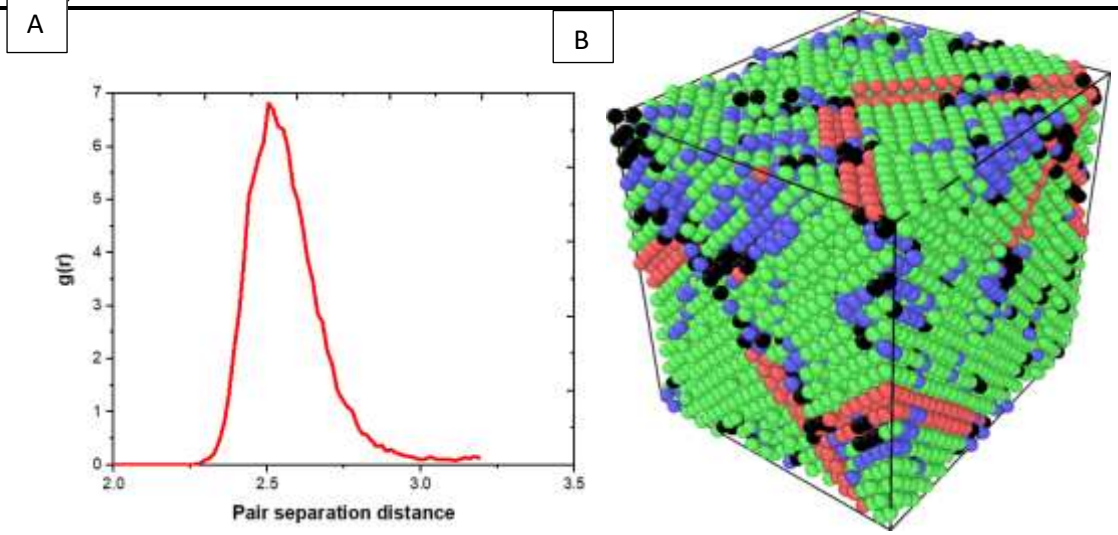

Figure 2. (a) The structural pair function, g®; (b) phase structure of the Al0.3CoCrFeNi HEA.

3.2. The Effect of Temperature

The **s**train -stress curves of our HEA are shown in Figure 3 for a strain rate of 1 x 10^{10} s^{-1} and range of temperature from 250 K to 1870 K. It is discovered that the elastic stress strain limit exists up to 2% strain, after which instability causes yielding and then plastic deformation. For Al0.3CoCrFeNi HEA, it has been discovered that fracture strain increases across the board as temperature rises. This indicates that AlxCoCrFeNi HEAs have a substantial reliance on temperature and is consistent with earlier similar experimental investigations [7]. The pace at which the stress decreases from a plateau in yield after yield stress, however, is slower the higher the temperature. From an energy standpoint, it is simple to comprehend that at higher temperature, the atoms' thermal motion will be high to migrate, which in turn weakens the HEAs' structural stability. As can be observed, the shear strain is primarily scattered throughout the shear zone and is minimal when the temperature is low. Due of the extremely localized deformation in the HEA. According to experimental findings by Wang et al. [8] annealing significantly improves the yielding strength and ultimate tension strength of Al0.3CoCrFeNi HEA, raising them to 870 MPa and 1060 MPa, respectively. This is a reliable sign that this alloy's partial recrystallization process resulted in a good strength-ductility combination. Another characteristic of Al0.3CoCrFeNi HEA is that it encompasses a remarkable variety of phase fields as a function of temperature, including the FCC, B2, L12, and BCC phases. It indicates that, after receiving the proper annealing treatment, this alloy composition is likely to separate into more than one phase. Due of the precipitates' potential role as barriers to dislocation motion, this presents a significant opportunity to increase the strength through fine-tuning the precipitate properties [8]. Table 1 provides the Young's modulus (E) at 250 K calculated from the linear slope of stress/strain curve in Figure 3. E and ρ are estimated to be 81 GPa and 7426 kg/m3, respectively. The characteristics of Al0.1CoCrFeNi HEA, which were discovered to have a value of E equals to 199 GPa and density 8018 kg/m^3 [18], are thus very similar to those of our alloy[12].

Table 1: Molecular simulation estimations for density (ρ) and Young's modulus (E) at 250 K are compared to published experimental findings.

Property	MD	Experiment
ρ(kg/m^3)	7426	7950[30]

E (GPa)	81	-

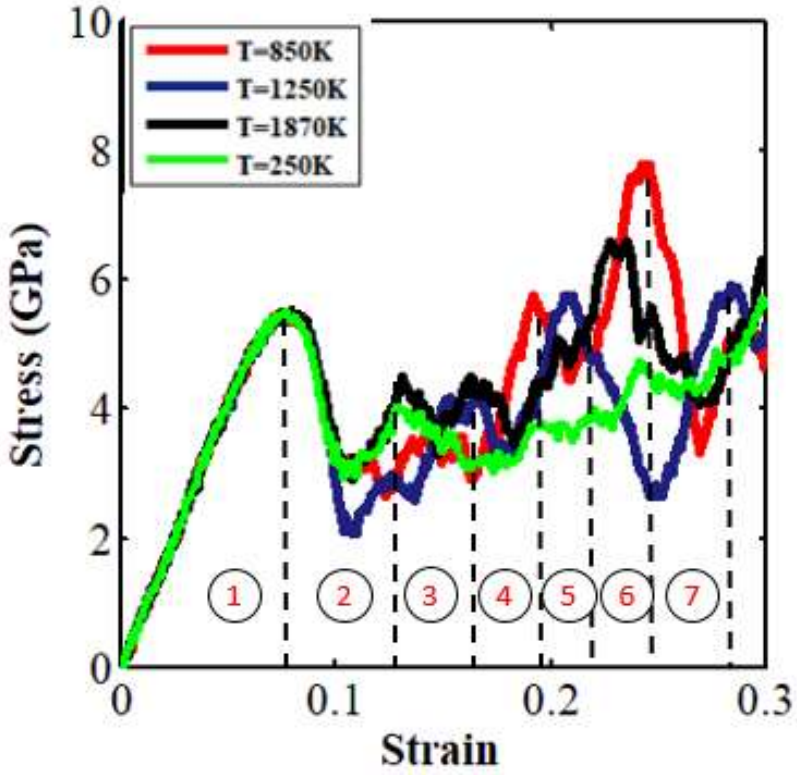

Figure 3. Depicts the stress-strain profiles of HEA at different temperatures.

3.3 The Effect of Strain Rate

By examining the stress-strain relationship of $Al_{0.3}CoCrFeNi$ HEAs at 250 K and strain rates of 10^8, 10^9, and $10^{10}s^{-1}$. The impact of strain rate on the compressive properties of the HEA has been focused on. According to Figure 4, at the same temperature, the yielding stress and strain of HEAs climb when the strain rate rise, but the elastic modulus of the alloy is not significantly affected. Heggen et al. [31] directly correlate strain rate and free volume, according to a study. A higher free volume can be attained by boosting the strain rate. At larger strain rates, however, the amount of time needed for rearranging the free volume and atom mobility will be drastically reduced. As a result, there will be less effective free volume, which influences atom migration during the process of deformation. As a result, the material's strength will increase and atom migration during deformation will become challenging. The Al0.3CoCrFeNi HEA's Young's modulus rises from 87.1 to 87.7 GPa when the strain rate rises from 10^8 to $10^{10}s^{-1}$.The yield stress climbs from 1.83 to 3.39 GPa, and the Young's modulus of the Al2.0CoCrFeNi rises from 39 to 42.18 GPa. It suggests that whereas the yield stress of the AlxCoCrFeNi HEAs is more influenced by the strain rate than the Young's modulus is. Additionally, the Young's modulus and yield strength of HEAs with greater Al contents are more significantly affected by the increase in strain rate. Higher strain rates of 10^8 10^{10}/s are used in MD simulations to produce a prediction within a realistic computed time due to the length and time scale limitations [32]. The experimentally attainable high strain rate (10^3/s) is now impossible due to this development. The yield strength might therefore exceed the experimental value as a result of this. The HEAs' deformation patterns seen in our investigation, however, are equivalent to those seen experimentally under high strain rates. Al0.6CoCrFeNi HEAs were

subjected to dynamic loading studies by Wang et al. [33] They discovered that raising the strain rate has no discernible effect on the yield strength.

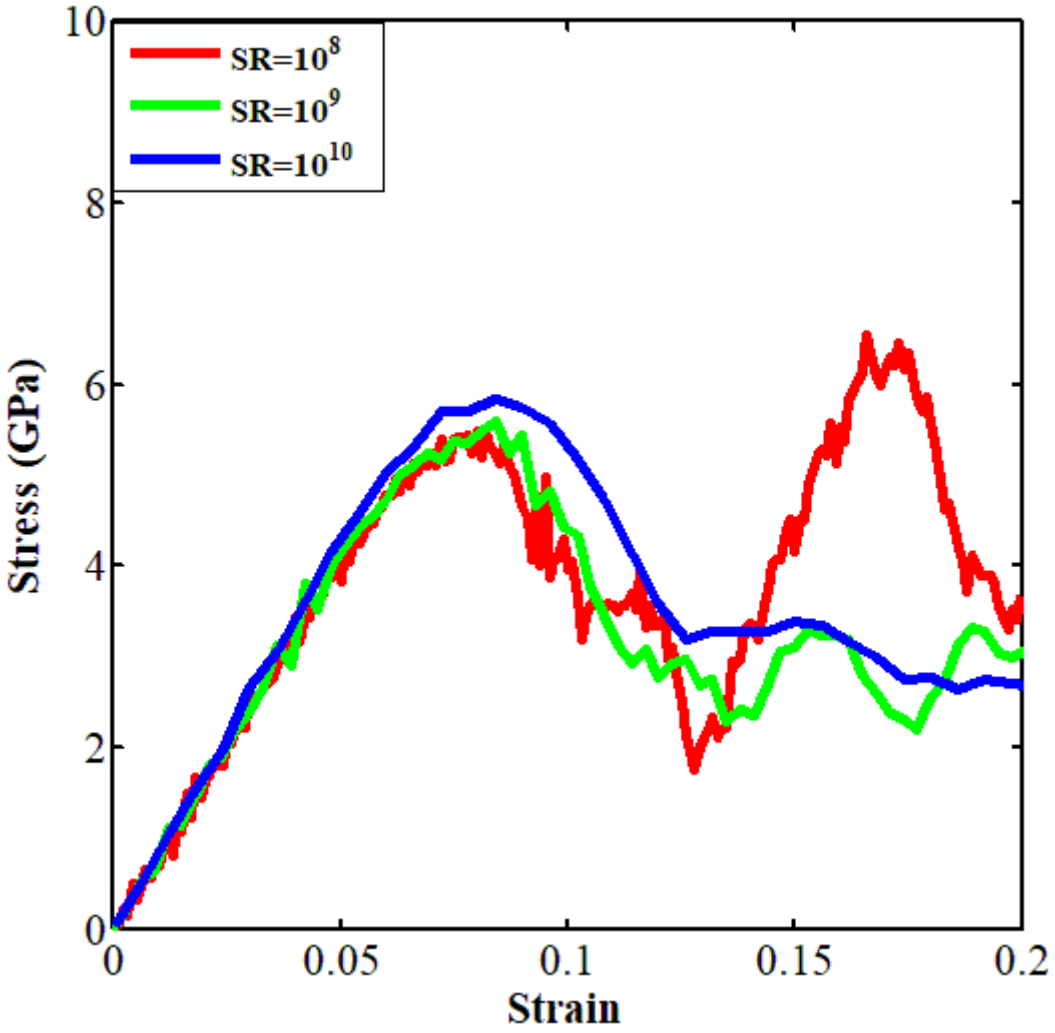

Figure 4. Illustrates the stress-strain trends of HEA at variant strain rates at 250K.

3.4 Dislocation Mechanism

Figure 5 depicts the various dislocations seen during compression loading of the HEA at several temperatures, including 250K, 850K, 1250K, and 1870K with a strain rate of $1x10^{10}s^{-1}$, based on the algorithm of dislocation extraction (DXA) [25], The segments of a dislocation are color-coded according to the type of dislocation: a blue line indicates a perfect dislocation, a green for a Shockley, a yellow for a Hirth, a magenta line a stair-rod dislocation, a cyan line a Frank, and a red line a different type of dislocation. From Figure 5, at 250 K, it can be seen that the Shockley and stair rod dominate all other forms of dislocation. At 850 K, Shockley and Hirth can be noticed to prevail. At 1250 K, it can observed that small percentages of Shockley and stair rods. At 1870 K, the three dislocations (Shockley, Hirth and stair rods) co-exist. As a result of the movement of Shockley partial dislocations during the beginning phases of deformation, stacking faults develop and vanish in a single phase, according to experimental reports [34]. So, in place of minimal strain hardening, the Shockley in the HEA accommodate the strain during the deformation and diminish dislocation storage. This discovery suggests that When there is a significant amount of Shockley dislocations present, the ability to boost the HEA strength with an elevation in strain hardening is greatly impeded[12].

Figure 6 illustrates the fluctuation of dislocation density (ρd) with strain at 250 K and 1870 K. The formula for determining the number of dislocations in an alloy is d = DL/V,

where DL is the whole length of the dislocation line and V is the volume of the simulation cell. The fact that d starts out at 5.1x 10^{17} m^2 for the 250 K scenario and 3.3 x10^{17} m^2 at 1870 K suggests that as temperature rises, dislocation motion is accelerated, leading to a drop in dislocation density as dislocation annihilation takes place. As a result, we discover that at 250 K, plastic deformation eliminates dislocations in the HEA, whereas at higher temperatures, strain hardening results from a boosting in dislocation density caused by the confined motion of the dislocations, which results in the formation of defects like new vacancies and dislocations. Evidently, the dislocation density rises as the strain does, demonstrating a direct connection between the development of dislocations and plastic deformation[14].

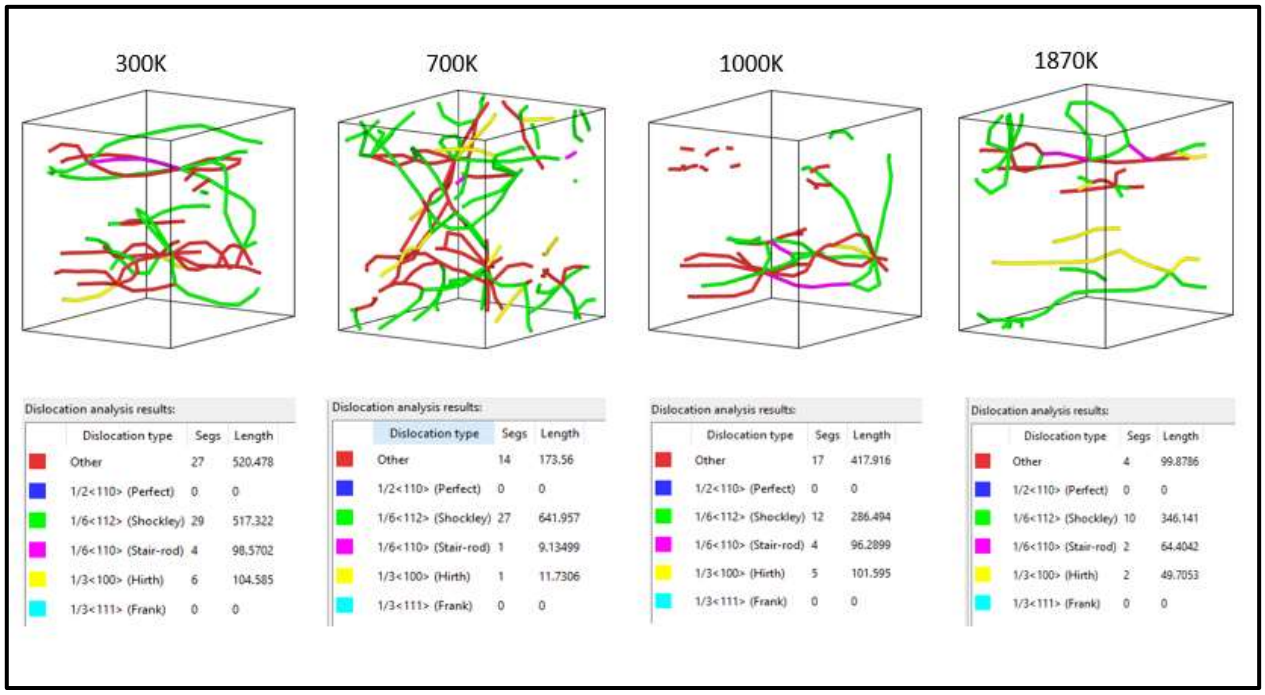

Figure 5. Demonstrates the dislocation progression of Al0.3CoCrFeNi at temperature levels of 250K, 850K, 1250K, and 1870K.

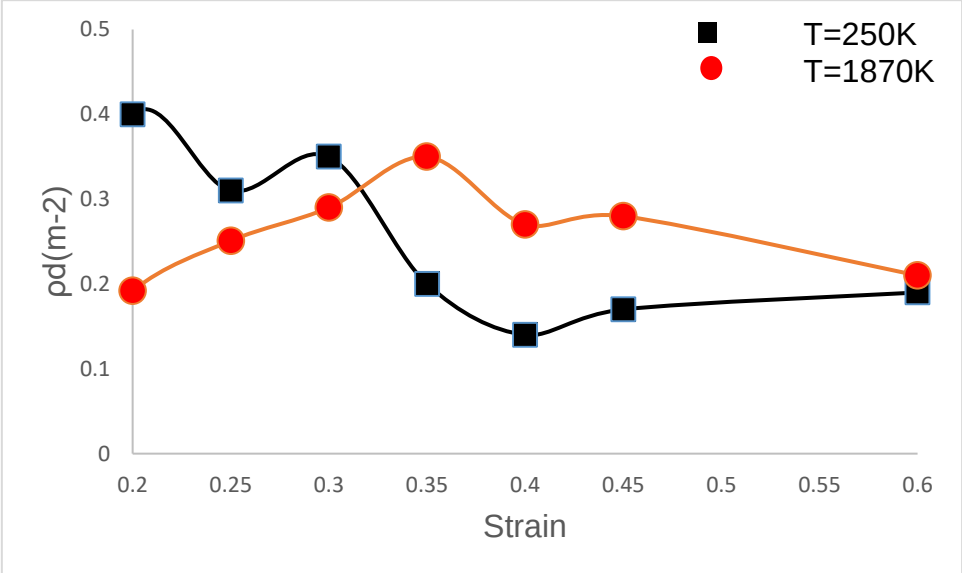

Figure 6. Dislocation density (ρd) for the Al0.3CoCrFeNi HEA at (250 & 1870K).

3.5 Phase Transformations

Schematic representation of the transition from FCC to HCP is displayed in Figure 7. For the deformed alloy at 250 –1870 K, CNA provides insights on deformation mechanisms including, twin boundaries (TBs),

both extrinsic and intrinsic stacking faults (SF), as shown in Figure 7. As it can be noted, the plastic deformation of the model during the plastic stage was primarily controlled by slippage, and stacking flaws were essential to the process[12]. The behavior of the stress fluctuation was discovered as a result of the development of stacking fault networks. Figure 7 depicts the interaction between dislocations and stacking faults when compressed. There is friction between the neighboring HCP ISFs as the model starts to slip for the second or third time under compression, and unlike friction in metal alone, this friction is quite distinct because of the difference in component radii. For smooth slippage, the friction between defects must be removed. During the sliding process, many challenges arise[14], Additionally, partial dislocation interactions result in other barriers that cause further hardness. Two dynamic incomplete dislocation components cooperating to create a three-dimensional body flaw in the stacking-fault structure. On the adjacent plane, a second Shockley incomplete dislocation creates the extrinsic stacking fault (ESF). According to ESF, two twin boundaries separate the twinned zone. It is noteworthy to note that in the simulation, the FCC structure does not automatically change into the HCP phase. Due to the typical low energy of ISF, an intermediate ISF product is required in the transformation. ISF has low energy, which contributes to the HCP production through ISF. The starting point of plastic deformation is no longer phase transformation, according to this finding [14].

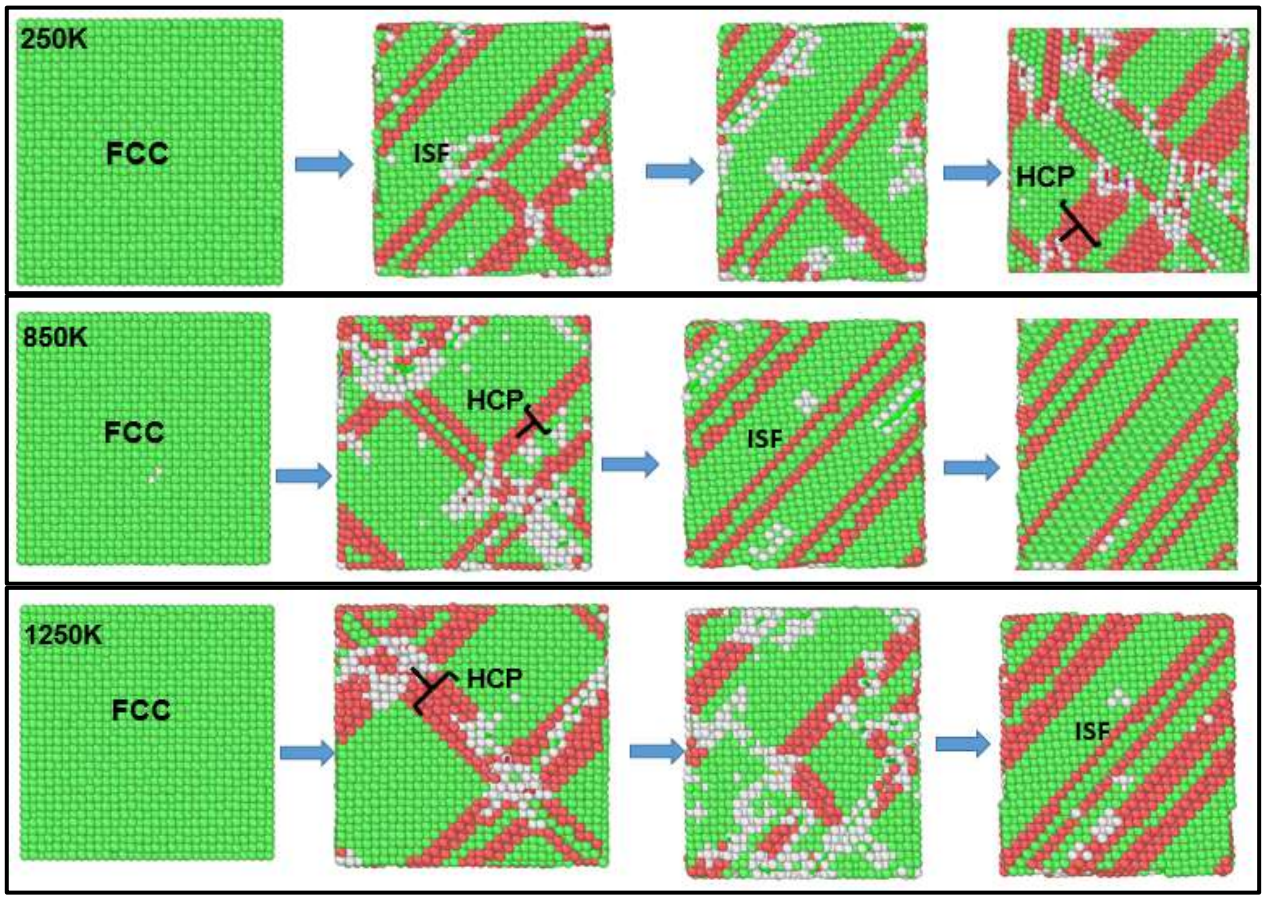

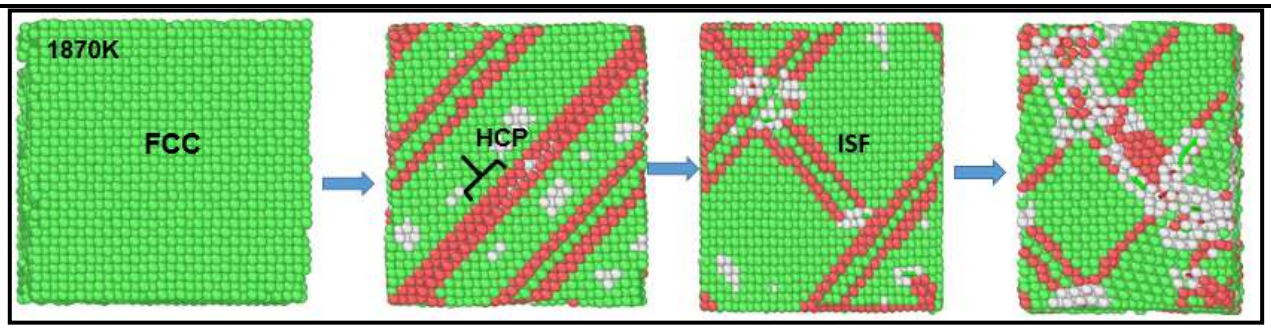

Figure 7. Atomic arrangements and the associated schematics for FCC to HCP phase transformations.

4. Conclusion

Using classical molecular dynamics computations, $Al_{0.3}CoCrFeNi$ high-entropy alloy has been studied. The phase transformations and dislocation mechanisms have been explored under various factors, such as a variety of temperatures between 250 K and 1870 K and different strain rates ranging from 10^8 to $1x10^{10}$ s^{-1} have been taken into account. It was deduced that A crucial aspect of the phase transformational process is stacking fault. For the case of high-entropy alloys, it is feasible to create stacking faults because of the presence of lattice distortion effect. According to the structure of FCC and HCP, phase transition with increasing strain from the primary form of FCC into BCC, HCP, and amorphous form, particularly after the yield strain through the introduction of stacking faults principles, which are consistent with the experimental observations. Furthermore, at low temperatures (250K), the Shockley and stair rods dominate all other forms of dislocation. At medium temperatures (850 K), Shockley and Hirth prevail. Moreover, at 1250 K, small percentages of Shockley and stair rods can be noted. At melting point (1870 K), Shockley, Hirth and stair rods dislocations co-exist. Stacking faults occur and dissipate in the single phase due to the migration of Shockley fractional dislocations at the initial phases of deformation. When the HEA deforms, the Shockley in the structure take up the strain. This discovery suggests that when Shockley dislocations are heavily present, the ability to enhance HEA strength with an upsurge in strain hardening is significantly hindered.

References:

[1] M. A. Hassan, H. M. Yehia, A. S. A. Mohamed, A. E. El-Nikhaily, and O. A. Elkady, "Effect of copper addition on the alcocrfeni high entropy alloys properties via the electroless plating and powder metallurgy technique," *Crystals*, vol. 11, no. 5, pp. 1–19, 2021, doi: 10.3390/cryst11050540.

[2] D. Li *et al.*, "High-entropy Al0.3CoCrFeNi alloy fibers with high tensile strength and ductility at ambient and cryogenic temperatures," *Acta Mater.*, vol. 123, pp. 285–294, 2017, doi: 10.1016/j.actamat.2016.10.038.

[3] M. Tokarewicz, M. Grądzka-Dahlke, K. Rećko, and M. Łępicka, "The Influence of Annealing at 500 and 900 °C on the Structure and Mechanical Properties of AlxCoCrFeNi Alloys," *Materials (Basel).*, vol. 16, no. 3, 2023, doi: 10.3390/ma16031245.

[4] P. M. Gopal, K. Soorya Prakash, V. Kavimani, and G. Rajendiran, "Processing and Properties of AlCoCrFeNi High Entropy Alloys: A Review," *Adv. Mater. Sci. Eng.*, vol. 2022, 2022, doi: 10.1155/2022/1190161.

[5] Y. Zhang, S. G. Ma, and J. W. Qiao, "Morphology transition from dendrites to equiaxed grains for AlCoCrFeNi high-entropy alloys by copper mold casting and bridgman solidification," *Metall. Mater. Trans. A Phys. Metall. Mater. Sci.*, vol. 43, no. 8, pp. 2625–2630, 2012, doi: 10.1007/s11661-011-0981-8.

[6] Z. M. Jiao, S. G. Ma, G. Z. Yuan, Z. H. Wang, H. J. Yang, and J. W. Qiao, "Plastic Deformation of Al0.3CoCrFeNi and AlCoCrFeNi High-Entropy Alloys Under Nanoindentation," *J. Mater. Eng. Perform.*, vol. 24, no. 8, pp. 3077–3083, 2015, doi:

10.1007/s11665-015-1576-0.

[7] T. T. Shun and Y. C. Du, "Microstructure and tensile behaviors of FCC Al0.3CoCrFeNi high entropy alloy," *J. Alloys Compd.*, vol. 479, no. 1–2, pp. 157–160, 2009, doi: 10.1016/j.jallcom.2008.12.088.

[8] X. Wang, Z. Zhang, Z. Wang, and X. Ren, "Microstructural Evolution and Tensile Properties of Al0.3CoCrFeNi High-Entropy Alloy Associated with B2 Precipitates," *Materials (Basel).*, vol. 15, no. 3, 2022, doi: 10.3390/ma15031215.

[9] B. Gwalani *et al.*, "Stability of ordered L12 and B2 precipitates in face centered cubic based high entropy alloys - Al0.3CoFeCrNi and Al0.3CuFeCrNi2," *Scr. Mater.*, vol. 123, pp. 130–134, 2016, doi: 10.1016/j.scriptamat.2016.06.019.

[10] J. Jiang *et al.*, "Microstructural evolution and mechanical properties of AlxCoCrFeNi high-entropy alloys under uniaxial tension: A molecular dynamics simulations study," *Mater. Today Commun.*, vol. 28, no. June, p. 102525, 2021, doi: 10.1016/j.mtcomm.2021.102525.

[11] A. Sharma, P. Singh, D. D. Johnson, P. K. Liaw, and G. Balasubramanian, "Atomistic clustering-ordering and high-strain deformation of an Al0.1 CrCoFeNi high-entropy alloy," *Sci. Rep.*, vol. 6, no. March, pp. 1–11, 2016, doi: 10.1038/srep31028.

[12] A. Sharma and G. Balasubramanian, "Dislocation dynamics in Al0.1CoCrFeNi high-entropy alloy under tensile loading," *Intermetallics*, vol. 91, no. July, pp. 31–34, 2017, doi: 10.1016/j.intermet.2017.08.004.

[13] Y. Afkham, M. Bahramyan, R. T. Mousavian, and D. Brabazon, "Tensile properties of AlCrCoFeCuNi glassy alloys: A molecular dynamics simulation study," *Mater. Sci. Eng. A*, vol. 698, pp. 143–151, 2017, doi: 10.1016/j.msea.2017.05.057.

[14] Y. Qi, H. Xu, T. He, M. Wang, and M. Feng, "Atomistic simulation of deformation behaviors polycrystalline CoCrFeMnNi high-entropy alloy under uniaxial loading," *Int. J. Refract. Met. Hard Mater.*, vol. 95, no. August 2020, p. 105415, 2021, doi: 10.1016/j.ijrmhm.2020.105415.

[15] S. Plimpton, "Fast Parallel Algorithms for Short-Range Molecular Dynamics for the United States Department of Energy under Contract DE.AC04-76DP00789," *J. Comput. Phys.*, vol. 117, pp. 1–19, 1995.

[16] "Daw, Murray S.; Mike Baskes (1984). 'Embedded-atom method: Derivation and application to impurities, surfaces, and other defects in metals'. Physical Review B. American Physical Society. 29 (12): 6443–6453".

[17] "O.R. Deluigi, R.C. Pasianot, F.J. Valencia, A. Caro, D. Farkas, and E.M. Bringa (2021), 'Simulations of primary damage in a High Entropy Alloy: Probing enhanced radiation resistance', Acta Materialia, 213, 116951. DOI: 10.1016/j.actamat.2021.1169".

[18] "R. Gröger, V. Vitek, and A. Dlouhý (2020), 'Effective pair potential for random fcc CoCrFeMnNi alloys', Modelling and Simulation in Materials Science and Engineering, 28(7), 075006. DOI: 10.1088/1361-651x/ab7f8b.".

[19] "I. Aslam, M.I. Baskes, D.E. Dickel, S. Adibi, B. Li, H. Rhee, M. Asle Zaeem, and M.F. Horstemeyer (2019), "Thermodynamic and kinetic behavior of low-alloy steels: An atomic level study using an Fe-Mn-Si-C modified embedded atom method (MEAM) pote".

[20] D. Farkas and A. Caro, "Model interatomic potentials for Fe–Ni–Cr–Co–Al high-entropy alloys," *J. Mater. Res.*, vol. 35, no. 22, pp. 3031–3040, 2020, doi: 10.1557/jmr.2020.294.

[21] D. F. Kadhim, M. V Koricherla, and T. W. Scharf, "Room and Elevated Temperature Sliding Friction and Wear Behavior of Al0.3CoFeCrNi and Al0.3CuFeCrNi2 High Entropy Alloys," *Crystals*, vol. 13, no. 4, pp. 1–12, 2023, doi: 10.3390/cryst13040609.

[22] A. Stukowski, "A. Stukowski, Modelling Simul. Mater. Sci. Eng. 18, 015012 (2010)," *Model. Simul. Mater. Sci. Eng.*, vol. 18, no. 1, p. 15012, Dec. 2009, doi: 10.1088/0965-0393/18/1/015012.

[23] J. D. Honeycutt and H. C. Andersen, "Molecular dynamics study of melting and freezing of small Lennard-Jones clusters," *J. Phys. Chem.*, vol. 91, no. 19, pp. 4950–4963, 1987, doi: 10.1021/j100303a014.

[24] "C.L. Kelchner, S. Plimpton, J. Hamilton, Dislocation nucleation and defect structure during surface indentation, Phys. Rev. B 58 (1998) 11085.".

[25] A. Stukowski and K. Albe, "Extracting dislocations and non-dislocation crystal defects from atomistic simulation data," *Model. Simul. Mater. Sci. Eng.*, vol. 18, no. 8, p. 85001, Sep. 2010, doi: 10.1088/0965-0393/18/8/085001.

[26] Y. F. Kao, T. J. Chen, S. K. Chen, and J. W. Yeh, "Microstructure and mechanical property of as-cast, -homogenized, and -deformed AlxCoCrFeNi (0 < x < 2) high-entropy alloys," *J. Alloys Compd.*, vol. 488, no. 1, pp. 57–64, 2009, doi: 10.1016/j.jallcom.2009.08.090.

[27] "Y. Zhang, T.T. Zuo, Y.Q. Cheng, and P.K. Liaw, High-Entropy Alloys with High Saturation Magnetization, Electrical Resistivity, and Malleability, Sci. Rep., 2013, 3, p 1455".

[28] W. R. Wang, W. L. Wang, and J. W. Yeh, "Phases, microstructure and mechanical properties of AlxCoCrFeNi high-entropy alloys at elevated temperatures," *J. Alloys Compd.*, vol. 589, pp. 143–152, 2014, doi: 10.1016/j.jallcom.2013.11.084.

[29] T. T. Shun, C. H. Hung, and C. F. Lee, "Formation of ordered/disordered nanoparticles in FCC high entropy alloys," *J. Alloys Compd.*, vol. 493, no. 1–2, pp. 105–109, 2010, doi: 10.1016/j.jallcom.2009.12.071.

[30] "K. Alagarsamy, A. Fortier, M. Komarasamy, N. Kumar, A. Mohammad, S. Banerjee, H.C. Han, R.S. Mishra, Cardiovasc. Eng. Technol. 7 (2016) 448.".

[31] M. Heggen, F. Spaepen, and M. Feuerbacher, "Creation and annihilation of free volume during homogeneous flow of a metallic glass," *J. Appl. Phys.*, vol. 97, no. 3, pp. 1–8, 2005, doi: 10.1063/1.1827344.

[32] "Sheng, H.F., & Peng, L.M. (2013). Microstructure and Tensile Properties of Al0.5CoCrCuFeNi High-Entropy Alloy. Applied Mechanics and Materials, 456, 494 - 497.".

[33] "L. Wang, J.W. Qiao, S.G. Ma, Z.M. Jiao, T.W. Zhang, G. Chen, D. Zhao, Y. Zhang, Z.H. Wang, Mechanical response and deformation behavior of Al0.6CoCrFeNi high-entropy alloys upon dynamic loading, Materials Science and Engineering: A, Volume 727, 2018, Page".

[34] "T.F. Yang, Z. Tang, X. Xie, R. Carroll, G.Y. Wang, Y.G. Wang, K.A. Dahmen, P.K. Liaw, Y.W. Zhang, Mat. Sci. Eng. A-Struct. 684 (2017) 552.".